Journal of Molecular Catalysis A: Chemical 347 (2011) 65–72

Contents lists available at ScienceDirect

Journal of Molecular Catalysis A: Chemical

journal homepage: www.elsevier.com/locate/molcata

Photocatalytic oxidation of salicylic acid and 4-chlorophenol in aqueous solutions mediated by modified $AlFe_2O_3$ catalyst under sunlight

S.S. Shinde, C.H. Bhosale, K.Y. Rajpure*

Electrochemical Materials Laboratory, Department of Physics, Shivaji University, Kolhapur 416004, Maharashtra, India

ARTICLE INFO

Article history:
Received 6 May 2011
Received in revised form 16 July 2011
Accepted 18 July 2011
Available online 23 July 2011

Keywords:
Nanocrystalline iron oxides
TiO_2
Photoelectrocatalysis
Organic impurities
Kinetic study

ABSTRACT

The visible light photochemical and photocatalytic oxidation of salicylic acid and 4-chlorophenol in a photoelectrocatalytic degradation reactor, at room temperature, under sunlight illumination, coated with anatase TiO_2-based Fe_2O_3 and $AlFe_2O_3$ photocatalysts were investigated. The solar radiation can effectively be applied to accelerate the process using suitable catalyst for economically cleaning the major fresh water sources. The profile of the oxidation of salicylic acid and 4-chlorophenol was followed by monitoring the target compound degradation, the total organic carbon removal and the mineralization process by chemical oxygen demand taking place during the oxidation with simultaneous conversion. Finally, based on the proposed mechanism a kinetic analysis was conducted in order to calculate the respective rate constants.

1. Introduction

Transition metal oxides have recently attracted a great interest in our aim to develop readily available, cheaper and more efficient catalysts as an alternative to traditionally employed noble metal catalysts in several catalytic reactions [1]. Among these transition metals, iron oxide (Fe_2O_3) has been explored as catalysts for a range of catalytic processes including oxidations [2], couplings [3] and alkylation-type processes [4]. Semiconductor photocatalysis is one of the advanced physicochemical processes applicable for photodegradation of environmental organic pollutants and toxins [5]. Also the various metal oxide semiconductor photocatalysts, anatase crystalline form of TiO_2 were intensively studied due to its biological and chemical inertness, non-toxicity, strong oxidizing activity and long-term chemical stability [6–8]. However, TiO_2 mainly absorbs UV light with wavelengths <380 nm (which covers only <3% of the solar spectrum) due to its wide band-gap of 3.2 eV. Therefore, it is of great interest to develop new visible light photocatalyst to enlarge the absorption wavelength range into the visible region. Fe_2O_3 with band-gap of 2.2 eV is an interesting n-type semiconducting material and a suitable candidate to be used as a photocatalyst in visible light. The photocatalytic nature of Fe_2O_3 has been investigated in water splitting [9], semiconductor electrode applications [10] and photodegradation of organic pollutants [11–15]. One of the ways to enhance visible light photocatalytic activity of TiO_2-based semiconductor photocatalysts is improvement of TiO_2 by doping non-metal elements, such as nitrogen [16], carbon [17], metal elements [18,19], carbon nanotubes [20,21] and other semiconductors having narrower band-gaps [22,23]. In addition, due to the narrow band-gap of Fe_2O_3, it can be utilized as a sensitizer of TiO_2 photocatalyst. When Fe_2O_3–TiO_2 composite thin films are irradiated with visible light, the electrons in the valence band of Fe_2O_3 are excited to the conduction band and leave holes in the valence band. Using formation of the built-in potential in Fe_2O_3–TiO_2 heterojunction, electrons in the valence band of TiO_2 are driven into Fe_2O_3 (while photogenerated holes move into the valence band of TiO_2 in an opposite direction). The charge transport between the valence bands of Fe_2O_3 and TiO_2 is considered as effective process for promoting the photocatalytic activity of the composition, because it results an increase in the electron–hole recombination time. In this regard, the photocatalytic activity of Fe-doped TiO_2 photocatalysts and Fe_2O_3–TiO_2 coupled semiconductor photocatalysts for photodegradation of toxic and organic pollutant substances in visible light have been recently investigated [24,25]. But, Fe_2O_3 itself does not show a high photocatalytic activity (as compared to TiO_2) may be due to its low charge carrier mobility and fast recombination or back reaction of the photogenerated pairs [26].

Salicylic acid, chlorophenols, dyes are noxious compounds which present in wastewater mainly arise from chemical intermediates or by-products in petrochemical, paper making, plastic, pesticidal, textile manufacturing and water disinfection. Moreover, salicylic acid and chlorophenols are one of the most vulnerable water pollutants, which cause serious damage to the vital

* Corresponding author. Tel.: +91 231 2609435; fax: +91 231 2691533.
E-mail address: rajpure@yahoo.com (K.Y. Rajpure).

1381-1169/$ – see front matter © 2011 Elsevier B.V. All rights reserved.
doi:10.1016/j.molcata.2011.07.012

organs of human beings [27]. Thus, the removal of the salicylic acid and chlorophenols from the wastewater is highly imperative. Literature gives the photocatalytic degradation of few organic impurities using ZnO, Fe_2O_3 and TiO_2 photocatalyst [20–29]. Unfortunately, there has been no report available on the degradation of salicylic acid and chlorophenols using TiO_2/Al:Fe_2O_3/FTO/glass. In this work, the visible light photocatalytic activity of the TiO_2/Fe_2O_3/FTO/glass thin film, as a photocatalyst for degradation of salicylic acid and 4-chlorophenol was investigated and compared corresponding activity to the Fe_2O_3 thin film. A mechanism for description of photocatalytic activity of the TiO_2/Fe_2O_3 and its improvement than the activity of the Fe_2O_3 thin film was also proposed.

2. Experimental

2.1. Catalyst preparation

Pure iron oxide and aluminium doped iron oxide photocatalysts were deposited on to fluorine doped tin oxide (FTO) glass substrates using chemical spray pyrolysis technique. The deposition method involved the decomposition of aqueous solution of high purity 0.1 M ferric trichloride (99.99%, A.R. grade, Himedia) using double distilled water as a solvent. To achieve, aluminium doping, A.R. grade aluminium nitrate was incorporated in to the ferric trichloride solution. Then resulting mixed solution was sprayed onto preheated substrates held at optimized substrate temperature of 623 K with compressed air as a carrier gas. Spray pyrolysis technique was utilized to deposit anatase TiO_2 coatings on the nanocrystalline Al:Fe_2O_3 thin films. Titanyl acetyl acetonate (TiAcAc) was used as a precursor for deposition of TiO_2 layer on to the Al based iron oxide films. The 10 cc solution of 0.1 M TiAcAc solution prepared in methanol was sprayed onto the iron oxide substrates keeping 470 °C substrate temperature. Other preparative parameters viz. spray rate: 5 cc min^{-1}, nozzle to substrate distance: 32 cm, nozzle diameter: 0.05 cm was kept constant for all experiments. Thickness of the TiO_2 coatings deposited on glass substrate was measured about 20 nm using surface profiler unit.

2.2. Catalyst characterization

The morphological characterization of photocatalyst was studied using atomic force microscopy (AFM, Digital Instrument, Nanoscope III) operated at room temperature. AFM images were collected in contact mode on a molecular imaging system using a silicon nitride cantilever. The chemical state of iron and its coordination were investigated by ^{57}Fe Mössbauer spectroscopy using a spectrometer (Nucleonix Systems Pvt. Ltd.) operated in constant acceleration mode (triangular wave) in transmission geometry. The source employed is Co-57 in Rh matrix of strength 50 mCi. The calibration of the velocity scale is done using a α-Fe metal foil. Spectra were recorded at room temperature (RT) within a velocity range −10 to +10 mm/s and the signal was transmitted to a multi-channel analyzer. The outer line width of calibration spectra is 0.29 mm/s. Data analysis involved a curve-fitting procedure made by a least square fit (MOSFIT) programme assuming Lorentzian line shapes.

2.3. Catalytic tests

Analytical reagent grade salicylic acid (C_6H_4(OH)COOH) and 4-chlorophenol or 4-CP (HOC_6H_4Cl) were obtained from Sigma–Aldrich and s.d. fine Chem. Ltd. Other chemicals such as potassium dichromate ($K_2Cr_2O_7$), sulphuric acid (H_2SO_4) and perchloric acid ($HClO_4$) all obtained from Loba Chemie were used with required concentrations without further purification. All the solutions were prepared using ultrapure water from Millipore water system (Milli-Q). The anatase TiO_2/Al:Fe_2O_3 electrodes used in this study were deposited by spray pyrolysis onto large area (10 cm × 10 cm) conducting glass plates (spray deposited fluorine doped tin oxide on glass, FTO, with sheet resistance of 10–20 Ω sq^{-1}). Preparation and structural, optical and photoelectrochemical characterization of the Al:Fe_2O_3 electrodes have been reported elsewhere [30–32] and typical optimized 10 at.% electrode was chosen in this study. Solar light was used as a source of illumination at a location of 16°40′37″N74°815′18″E.

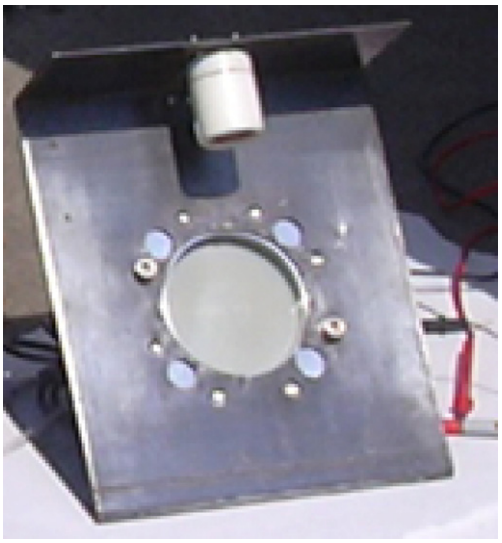

Fig. 1. Experimental setup of photoelectrocatalytic degradation reactor.

The appropriate concentrations of salicylic acid and 4-CP were used as model pollutants in water for degradation studies under solar light illumination in the presence of TiO_2/Al:Fe_2O_3 photocatalyst. A fixed amount of electrolyte, the major part of which contained in an external reservoir, was recirculated through the photoelectrochemical cell with a constant flow rate of 8.4 l h^{-1} (flow velocity 2.92 cm s^{-1}) using a Gilson MINIPLUS peristaltic pump, France with silicon tubing. The experimental setup of photoelectrocatalytic degradation reactor is as shown in Fig. 1. Using aliquots withdrawn from the reaction mixture at some intervals, the concentrations of organic impurities in the solutions were determined by measuring the UV–Vis absorbance (extinction) using a 119 SYSTRONICS UV–vis spectrophotometer (for the measurement of full spectra). The absorbance (extinction) was measured in 1 cm quartz cell at particular wavelength (where maximum absorption peak is observed) for various impurities. Total organic carbon (TOC) concentration represents the mineralization extent of organic substances in water. TOC was measured using the aliquots after acidification with phosphoric acid and purging out IC (inorganic carbon, CO_2) by catalytic combustion, using a Photometer model 400D. Aliquots extracted from the solutions at various intervals during the degradation reaction were also used for determining chemical oxygen demand (COD) using the standard method of oxidation with an excess of dichromate in concentrated sulphuric acid by digestion at 140 °C. The concentration of the organic solute was calculated from the dichromate extinction at various wavelengths.

3. Results and discussion

3.1. Surface morphological study

The two-dimensional atomic force microscopy (AFM) images of pure and typical 10 at.% Al:Fe_2O_3 catalysts are shown in Fig. 2(a

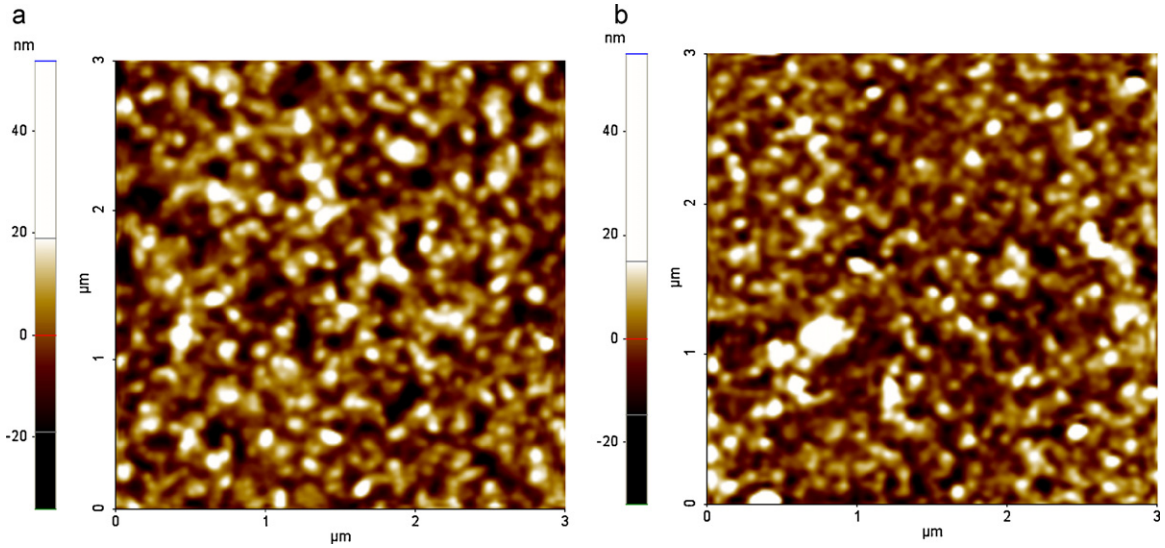

Fig. 2. Atomic force microscopic images of pure Fe_2O_3 and typical 10 at.% Al doped Fe_2O_3 thin films.

and b). The images were recorded on 1 μm × 1 μm planar in contact mode at the scan rate of 10.17 Hz. The micrograph shows that the catalysts are compact, adherent, homogeneous and large surface area with twisted spindle-shaped nanostructured grains without any feature on the surface. From the images, it is confirmed that films are converting from the microcrystalline to nanocrystalline form. In addition, out diffusion and subsequently agglomeration of the iron oxide atoms resulted in the formation of twisted chains of iron oxide grains with the grain size of 20–60 nm on the film surface. Therefore it can be concluded that the observed morphology boost suitable enhancement in efficiency of degradation for different organic species. Elsewhere, using AFM analysis, it was shown that the activation energy required for the formation of such form of Fe_2O_3 nanograins on the film surface is 0.55 eV, independent from the tip convolution effect [33]. The anatase TiO_2 layer was coated on surface of the $AlFe_2O_3$ catalysts shown in figure. But, in this work, we could not provide a suitable image to illustrate the TiO_2 coating on the Fe_2O_3 film. Therefore, we can assume that the uneven component distribution of $AlFe_2O_3$ which grown at relatively low concentrations could result in local sites with high strain.

3.2. Mössbauer spectroscopic analysis

Fig. 3(a and b) shows the room temperature Mössbauer spectra of pure and typical 10 at.% Al based iron oxide photocatalysts. It exhibits an asymmetrical sextet with broadened lines and a quadrupolar component: such hyperfine structure suggests the presence of static magnetic ordering and super paramagnetic relaxation phenomena originating from a distribution of size and/or distances between particles giving rise to an assembly of weakly interacting particles. The hyperfine structure of the Mössbauer spectra having the highest saturation magnetization consists of broad line sextet, which has to be described by at least three magnetic components with large line widths. Observed spectra show three sextet and one doublet phases in the deposited photocatalyst. The broadening enhances after Al doping in all sextets and doublets. The asymmetry of outermost lines has to be decomposed into at least two magnetic components, the hyperfine parameters of which are listed in Table 1. Also it shifts toward the lower velocity side due to doping influence. Also peak strength enhances after Al doping concentration due to the contribution of nanocrystalline Fe oxide species. The Mössbauer parameters are very close to the parameters of $AlFeO_3$ phase and iron is present in high spin Fe^{3+} state [34] reveals that the doped Al atom at intestinal position in the crystal. The QS values increases from 0.0773 to 0.0800 mm/s for first sextet attributing asymmetry around the iron ions. Magnetic hyperfine field (516.79–513.97 kG) and isomer shift (0.4508–0.4483 mm/s) values decreases with Al doping concentration for all sextets. This information was inferred from QS values which reflect variations of the electric field gradient felt by iron atoms thus giving valuable information on chemical and geometrical environment [35]. The presence of a doublet at room temperature can be related either to "isolated" Fe cations, for which only long-range dipolar interaction exists between Fe cations forming, spin fluctuations [36].

3.3. Photocatalytic activity

The photocatalytic activity of salicylic acid is investigated by exposing the salicylic acid solution to sunlight in the absence and in the presence of $AlFe_2O_3$ and $TiO_2/AlFe_2O_3$ photocatalyst. The salicylic acid does not undergo any degradation under direct visible (sunlight) irradiation in the absence of $TiO_2/AlFe_2O_3$. In the presence of $TiO_2/AlFe_2O_3$ and in the absence of sunlight, the salicylic acid is stable though adsorption was found to be responsible for small decrease in salicylic acid concentration under specified conditions. However, on irradiation with sunlight in the presence of $TiO_2/AlFe_2O_3$ the salicylic acid is almost completely degraded as shown in Fig. 4(a–d).

The photocatalytic degradation follows a pseudo first order reaction and its kinetics can be expressed using relation,

$$\ln\left(\frac{c}{c_0}\right) = -kt \quad (1)$$

where t is the time, k can be taken as the apparent first order rate constant of the degradation reaction; c stands for the concentration of the solute or the concentration of oxidizable atoms in the organic species; c_0 the initial concentration of solute, when COD is used. The rate constant in a batch reactor of given electrode size is inversely proportional to the volume. Moreover, k is proportional to the area of the electrode if a sufficiently well collimated light source is used and to its intensity and therefore to the photocurrent. In order to intangible from these external parameters and to make comparison of experimental data obtained under various conditions possible, it is useful to define,

$$k' = kV\,(\mathrm{cm}^3\ \ \mathrm{s}^{-1}) \quad (2)$$

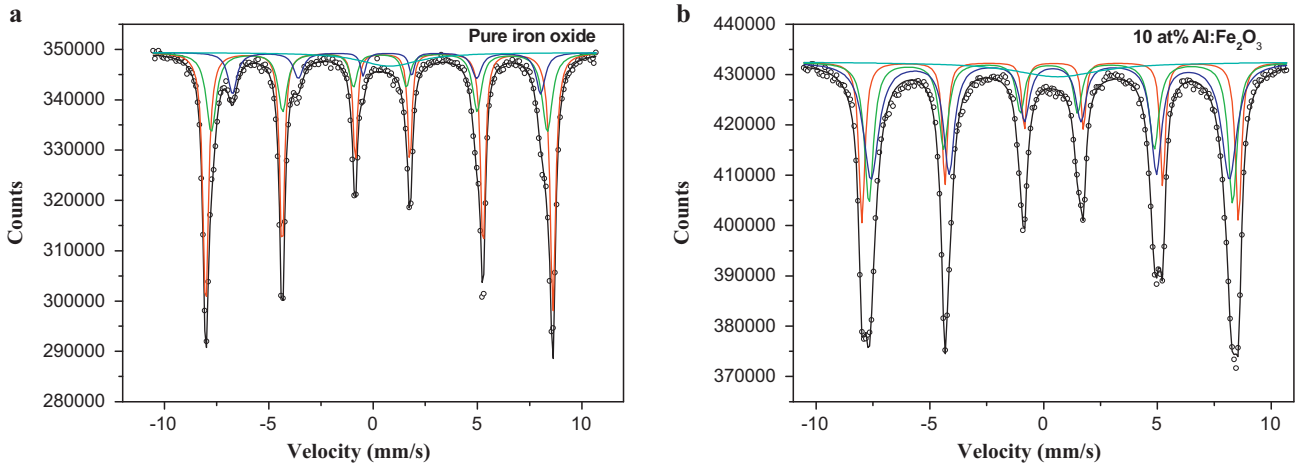

Fig. 3. (a and b) Mössbauer spectra of pure Fe_2O_3 and typical 10 at.% Al doped Fe_2O_3 thin films.

Table 1
The variation of hyperfine field, quadrupole splitting, isomer shift, outer line width and relative intensity are relative to Fe-metal foil of Fe_2O_3 and 10 at.% Al:Fe_2O_3 photocatalyst.

Sample	Phases	Hyperfine field, H_{int} (kG)	Quadrupole splitting, QS (mm/s)	Isomer shift, IS (mm/s)	Outer line width, Γ (mm/s)	Relative intensity, RI (%)
Pure iron oxide	Sextet 1 (red)	516.79	0.0773	0.4508	0.3150	51.01
	Sextet 2 (green)	500.11	0.014	0.3224	0.5710	28.25
	Sextet 3 (blue)	458.75	0.0227	0.6872	0.5157	13.35
	Doublet (cyan)	–	0.0211	0.7979	3.4435	07.39
10 at.% Al:Fe_2O_3	Sextet 1 (red)	513.97	0.0800	0.4483	0.3150	22.13
	Sextet 2 (green)	496.53	0.0416	0.2336	0.4710	29.19
	Sextet 3 (blue)	489.11	0.0564	0.4005	0.8080	41.22
	Doublet (cyan)	–	0.0583	0.6138	4.6242	7.46

$$k'' = \frac{k'}{A}\,(\mathrm{cm\ \ s^{-1}}) \tag{3}$$

$$p = k''' = \frac{kVF}{i_{ph}}\ \ (\mathrm{M^{-1}}) \tag{4}$$

where F is Faraday's constant (96,500 mol^{-1}), V the volume, A is the area of electrode, p or k'' the rate constant or kinetic parameter, which is independent of total photocurrent, i_{ph}, and total liquid volume. The p reflects the efficiency of oxidative degradation of the solute (when extinction is used) or of the amount of oxidizable atoms in the solution (in the case of COD).

Fig. 4(a) shows the augmentation of photocurrent as a function of reaction kinetic time during photo-degradation of salicylic acid. Although photocurrent decays over the course of time, an average of 0.013 A photocurrent is drawn from degradation of salicylic acid using Fe_2O_3, TiO_2/Fe_2O_3, $AlFe_2O_3$ and $TiO_2/AlFe_2O_3$ photocatalysts. The decrease in photocurrent in later stages of the experiment was due to the natural decrease in sunlight intensity in the afternoon as well as degradation of organic species. Fig. 4(b) shows the changes in the extinction spectra of salicylic acid collected at various intervals during its photoelectrochemical degradation recorded in the wavelength range from 200 to 350 nm. As a general trend, the extinction of all three bands in the UV (labelled A–C starting from around 200 nm) decreases with illumination time, but close inspection, e.g. in the region between the B- and the C-band, shows that the extent of this decrease is not the same for all wavelengths, hinting at the absorption by intermediate compounds. Visual inspection shows that after about 1 h of degradation reaction, the originally colourless solution becomes yellow. This could be due to formation of intermediate compounds in the reaction mixture. This coloration however disappears entirely after 1.5 h from start of the reaction. During the course of the degradation experiments, the concentration of salicylic acid decreases due to its photoelectrochemical oxidation. The degradation kinetics [plot of $\ln(ext/ext_0)$ as a function of reaction time] of salicylic acid is as shown in Fig. 4(c). The photocatalytic degradation of salicylic acid obeys first order kinetics (extinction taken at 306 nm). The linear portion in this plot has a slope of rate constant ($-k$). As illustrated in Fig. 4(c), the photocatalytic activities of nanocrystalline pure Fe_2O_3, TiO_2/Fe_2O_3, $AlFe_2O_3$ and $TiO_2/AlFe_2O_3$ photocatalysts are investigated on the photodegradation of salicylic acid under sunlight illumination. The comparison of various degradation kinetics parameters for different photocatalyst modifications for salicylic acid is shown in Table 2. The first order rate constant increases with respect to modification in photocatalysts. The value of k increases from 0.788 to $9.12 \times 10^{-4}\ s^{-1}$. Increase in the thickness of the TiO_2 layer results in decrease of the photocatalytic activity due to increase in distance of the electron–hole transfer from the interface to surface of the films. On the other hand, decrease in amount of the TiO_2 can reduce the effective surface of the TiO_2 and/or the interface area of the films containing the Ti–O–Fe bond.

The better photocatalytic performance of the Al:Fe_2O_3 than the TiO_2 photocatalyst thin film can be assigned in principle to considerable generation of electron–hole pairs through the narrow band-gap illumination of the Al:Fe_2O_3 thin film, which can be expressed as follows:

$$AlFe_2O_3 + h\nu \rightarrow AlFe_2O_3\ (e^-_{cb}, h^+_{vb}) \tag{5}$$

The effect of the excited electrons ($e_{cb}{}^-$) on promotion of the catalytic activity can be explained by the following two fold mechanisms [14]:

1. The excited electrons are directly trapped by the H_2O_2 of the solution to produce OH radicals, i.e.

$$H_2O_2 + e^-_{cb} \rightarrow OH^- + OH^\bullet \tag{6}$$

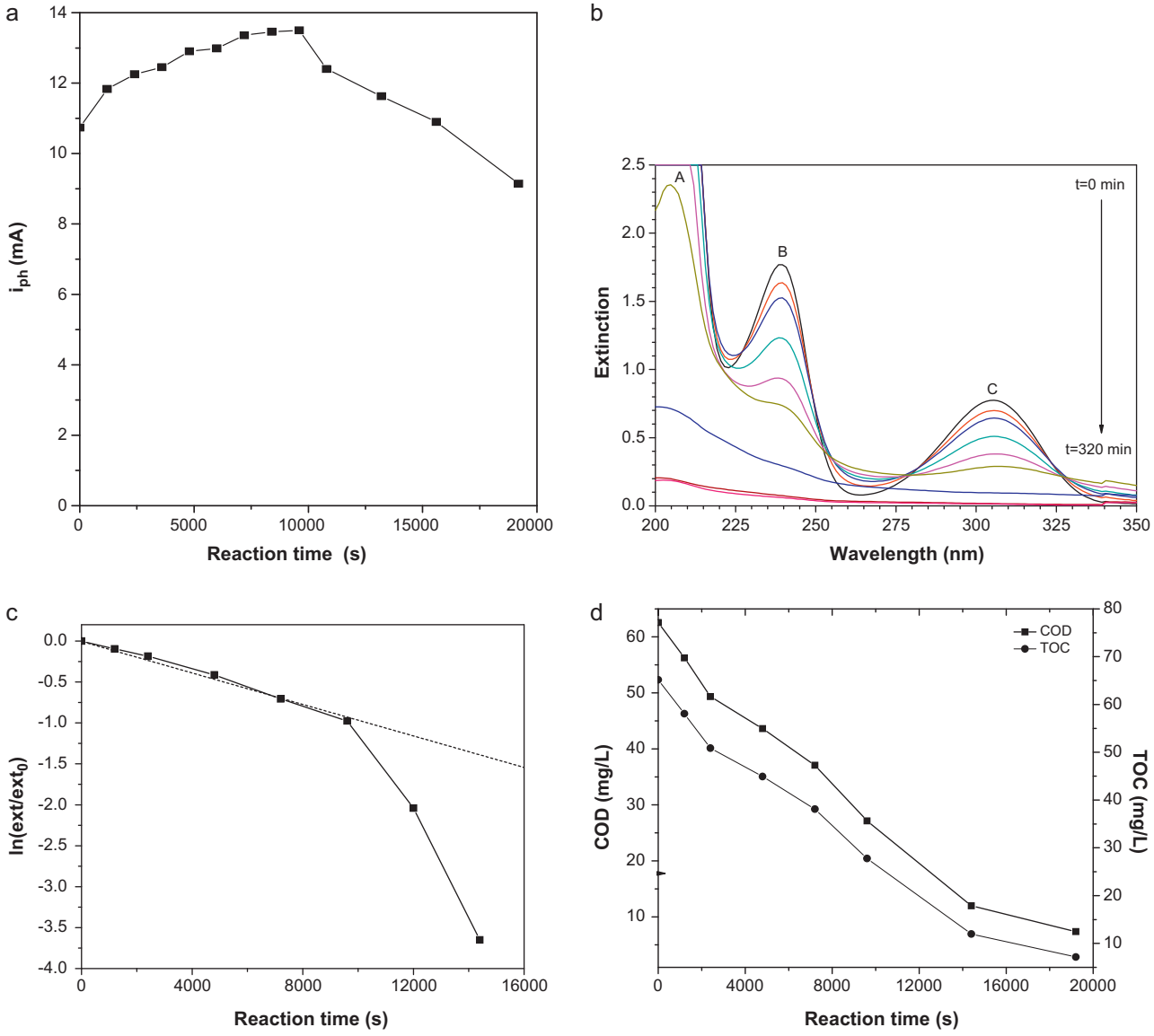

Fig. 4. Salicylic acid degradation on TiO_2/Al:Fe_2O_3 under sunlight illumination (a) plot of photocurrent as a function of reaction time, (b) extinction spectra with illumination time as parameter, (c) kinetics of degradation (extinction taken at 306 nm) and (d) extent of mineralization by COD and TOC.

Table 2
Various parameters and conditions for degradation of salicylic acid and 4-chlorophenol by Fe_2O_3, typical 10 at.% Al:Fe_2O_3, TiO_2/Fe_2O_3, and TiO_2/Al:Fe_2O_3 photocatalysts.

Solution	Bias or potential (V)	k (s^{-1}) (10^{-4})	$k' = kV$ ($cm^3\ s^{-1}$)	Active surface area (cm^2)	$k'' = k'$/area (10^{-3} cm s^{-1})	i_{ph} (A)	$k''' = kVF/i_{ph}$ (M^{-1})	$p = 1/k'''$ (M)
250 ml 1 mM Salicylic acid 10 mM $HClO_4$ (pure Fe_2O_3)	1.4 (photovoltaic silicon solar cell)	0.788	0.0197	64	0.307	0.013	146	0.0068
250 ml 1 mM Salicylic acid 10 mM $HClO_4$ (20 nm TiO_2 + pure Fe_2O_3)	1.4 (photovoltaic silicon solar cell)	0.567	0.0142	64	0.222	0.011	124	0.0081
250 ml 1 mM Salicylic acid 10 mM $HClO_4$ (10 at.% Al:Fe_2O_3)	1.4 (photovoltaic silicon solar cell)	1.11	0.0278	64	0.434	0.013	206	0.0048
250 ml 1 mM Salicylic acid 10 mM $HClO_4$ (20 nm TiO_2 + 10 at.% Al:Fe_2O_3)	1.4 (photovoltaic silicon solar cell)	9.12	0.228	64	3.56	0.0125	1760	0.00056
250 ml 1 mM 4-Chlorophenol 10 mM $HClO_4$ (10 at.% Al:Fe_2O_3)	1.4 (photovoltaic silicon solar cell)	1.44	0.036	64	0.563	0.015	231.6	0.0043
250 ml 1 mM 4-Chlorophenol 10 mM $HClO_4$ (20 nm TiO_2 + 10 at.% Al:Fe_2O_3)	1.4 (photovoltaic silicon solar cell)	6.23	0.156	64	2.44	0.018	830	0.0012

They are trapped, at first, by the surface Fe^{3+} leading to Fe^{2+} in the following reaction:

$$Fe^{3+} + e^{-}_{cb} \rightarrow Fe^{2+} \quad (7)$$

Then the Fe^{2+} can contribute in the reaction to produce OH radicals as follows [37]:

$$Fe^{2+} + H_2O_2 \rightarrow Fe^{3+} + OH^- + OH^{\bullet} \quad (8)$$

Oxidation ability of the reaction (8) can be greatly enhanced via the following reaction,

$$Fe^{3+} + OH^- + h\nu \rightarrow Fe^{2+} + OH^{\bullet} \quad (9)$$

Meanwhile, production rate of hydroxyl radicals can be enhanced by the stimulation of Fe^{2+} ions. The OH radicals ($OH^{\bullet}$) photogenerated from reactions (6), (8) and (9) are the main factors for degradation of the organic impurities in water. By deposition of the TiO_2 coating on the $AlFe_2O_3$ films, i.e. for the $TiO_2/AlFe_2O_3$ thin film, the rate of kinetics is measured, indicating a better performance than the bare Fe_2O_3 thin film in the same conditions, respectively. The better photocatalytic performance of the $TiO_2/AlFe_2O_3$ than the $AlFe_2O_3$ nanograins in the visible light irradiation can be assigned to the formation of $TiO_2/AlFe_2O_3$ heterojunction. When the heterojunction is irradiated by visible light, electrons in the valence band of $AlFe_2O_3$ are excited to the conduction band and leave holes in the valence band. Therefore, due to the built-in field in Fe_2O_3–TiO_2 heterojunction, electrons in the valence bands of TiO_2 are driven into the valence band of Fe_2O_3, while photogenerated holes moved into the valence band of TiO_2 in an opposite direction [25]. In addition to the reactions which produce OH radicals in presence of the $AlFe_2O_3$ catalyst, the TiO_2 coating in the $TiO_2/AlFe_2O_3$ could be effective in improvement of the photocatalytic activity of the coated $AlFe_2O_3$ films based on the following reactions:

$$Fe_2O_3\ (e^{-}_{cb}, h^{+}_{vb}) + Ti^{4+} \rightarrow Fe^{2+} + Ti^{4+}\ (h^{+}_{vb}) \quad (10)$$

This means that the TiO_2 could promote formation of Fe^{2+} to react with organic species of the solution and so the production of OH radicals. Furthermore, the holes can be trapped by water or hydroxyl groups adsorbed on the surface of the TiO_2 layer to generate active hydroxyl radicals for more degradation of organic impurities.

The salicylic acid solution is analyzed for COD and TOC measurements for extent of complete degradation as shown in Fig. 4(d). COD study as a function of reaction time provides the concentration of oxidizable matter left in the electrolyte solution. The COD values decreases from 62.57 to 7.38 mg L^{-1} with reaction time. It could be concluded that the suppression of electron–hole recombination and generation of more $^{\bullet}OH$ radicals in samples play an important role in the enhanced rate of photo mineralization. The observed decay constants indicate the destruction of main elements of salicylic acid. All the organic components were oxidized quantitatively to carbon dioxide as indicated by TOC determination. Carbon dioxide determined experimentally was found to tally with the theoretical values on the basis of molecular weight and concentration of the salicylic acid employed. TOC decreases from 65.17 to 7.17 mg L^{-1}, i.e. it shows ≈98% degradation of salicylic acid confirming almost complete mineralization of salicylic acid. From this result, it is concluded that the $TiO_2/AlFe_2O_3$ is the best reliable photocatalyst for degradation of salicylic acid.

Fig. 5 explains the 4-chlorophenol (4-CP) degradation on $TiO_2/AlFe_2O_3$ photocatalyst under sunlight illumination (a) plot of photocurrent as a function of degradation time, (b) optical absorption spectra with illumination time as parameter, (c) kinetics of degradation (extinction taken at 227 nm) and (d) degree of mineralization by COD and TOC. Fig. 5(a) shows the variation photocurrent as a function of time during degradation of 4-CP. A steadier average photocurrent of 0.018 A was drawn during 4-CP degradation experiment. The increase of concentration of intermediate products, as seen in the absorption spectra (Fig. 5(b)) is even more pronounced than in the case of salicylic acid. Based on the data acquired by the experiments performed in this study a kinetic analysis of the 4-CP using $AlFe_2O_3$ and $TiO_2/AlFe_2O_3$ catalysts is depicted. The possible reactions during degradation of 4-CP is:

$$C_6H_5ClO + OH^- + OH^{\bullet} \xrightarrow{h\nu} I \quad (11)$$

$$I + OH^- + OH^{\bullet} \xrightarrow{h\nu} CO_2 + H_2O + HCl \quad (12)$$

$$I + OH^- + OH^{\bullet} \xrightarrow{h\nu} CO_2 + H_2O \quad (13)$$

where I represents the total chlorinated organic intermediates.

The kinetic parameters have been evaluated at the 227 nm wavelength peak as shown in Fig. 5(c). The degradation of 4-CP under the experimental conditions of the study agreed remarkably to first-order kinetics. The applicability of the first-order kinetics to this study has been confirmed by the linearity of the plot of $\ln(c/c_0)$ against irradiation time for various experiments. The kinetic parameter k increases from 0.144 to 0.623×10^{-3} s^{-1} with respect to modification in (from $AlFe_2O_3$ to $TiO_2/AlFe_2O_3$) photocatalyst composition. The rate constant k'' increases from 231 to 830 M^{-1}. Extent of mineralization of the 4-CP can be evaluated by measuring TOC and COD measurement as shown in Fig. 5(d). The amount of COD of 4-CP has been reduced from 52 to 17.62 mg L^{-1} and TOC from 48 to 14.79 mg L^{-1}. The TOC concentration of 4-CP decreases significantly with increasing the irradiation time is as shown in Fig. 4(d). As irradiation time increases, 4-CP degrades into small fragments and consequently complete mineralization is achieved under $TiO_2/AlFe_2O_3$ photocatalyst. This is due to suppression of electron–hole recombination and generation of more $^{\bullet}OH$ radicals. The $^{\bullet}OH$ radicals are strong enough to break different (C–C, C–Cl, and C–O) bonds in 4-CP molecules adsorbed on the surface of Fe_2O_3 and this will lead to the formation of CO_2, H_2O and harmless inorganic ions. Upon illumination of aqueous semiconductor particles with light of sufficient energy, charge separation is induced resulting in the formation of valence band holes and conduction band electrons. These charge carriers may participate in the formation of active oxidizing species such as hydroxyl radical, hydroperoxyl radical, hydrogen peroxide and superoxide ions. Several literature studies attributed the oxidation of organic compounds mainly due to positive hole and/or hydroxyl radical ions [38]. Based on quantum yield study the oxidative mechanism over semiconductor ought to proceed via positive hole. However, there are convincing experimental proofs that both valence band hole and hydroxyl radical are involved in oxidative conversions of organic compounds on semiconductor photocatalysts [39]. More specifically, hydroxyl radicals has been shown to be the major oxidant involved in 70–90% of the photo-oxidation of organic compounds notably chlorophenols [40].

3.4. Reusability of photocatalyst

Reusability of $TiO_2/AlFe_2O_3$ and Al:Fe_2O_3 photocatalyst for the degradation of salicylic acid and 4-CP was estimated. The solution resulting from the photocatalytic degradation of the salicylic acid and 4-CP was filtered, washed and the photocatalyst was dried. The dried catalyst samples were used for the degradation of organic impurities under similar conditions. The filtrate was subjected to AAS analysis to assess the loss of photocatalyst ions in solutions but it did not show any sign of deterioration of TiO_2/Al:Fe_2O_3 photocatalyst. The photocatalyst TiO_2/Al:Fe_2O_3 could be used repeatedly

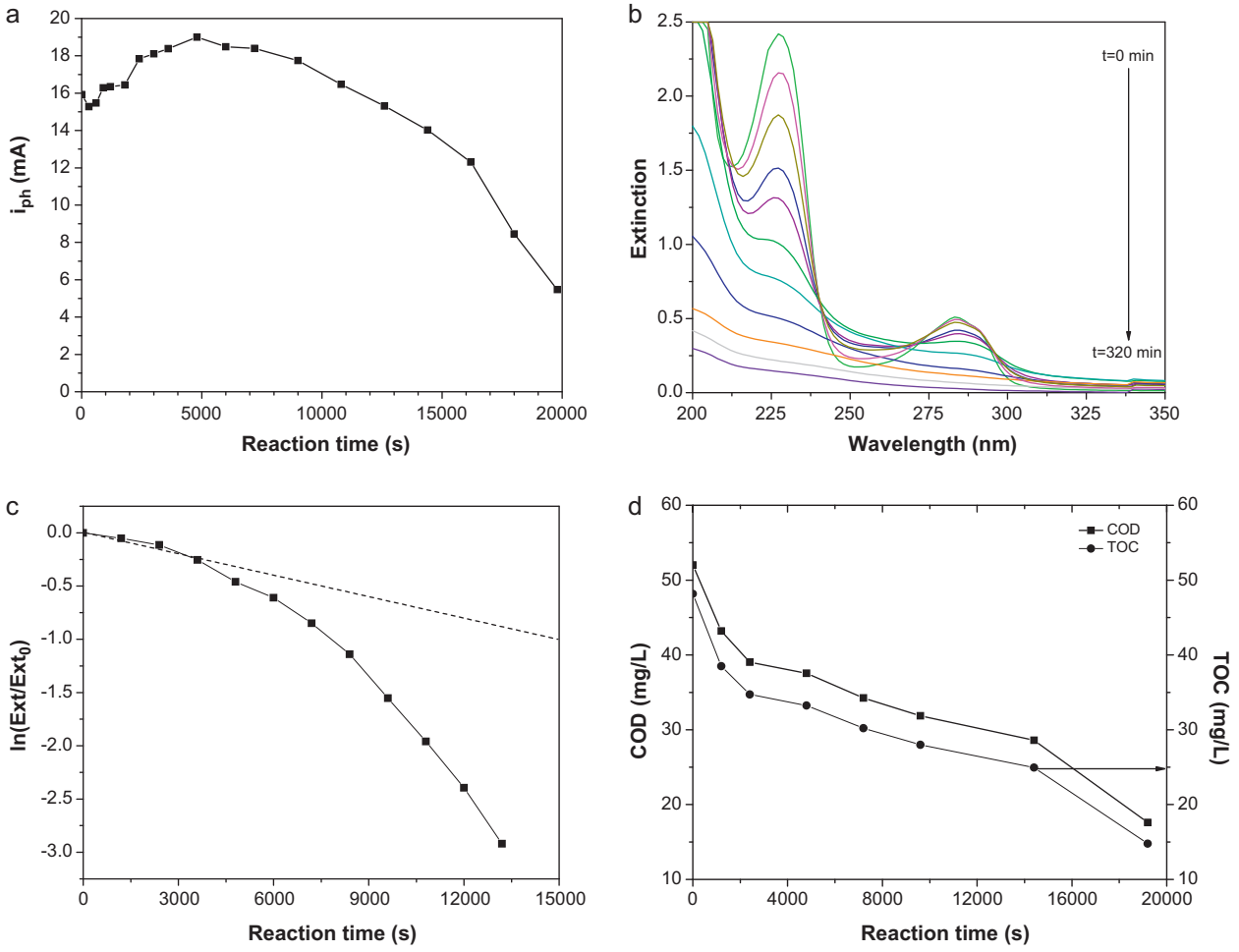

Fig. 5. Degradation of 4-chlorophenol (4-CP) on TiO_2/Al:Fe_2O_3 under sunlight irradiation (a) plot of photocurrent as a function of reaction time, (b) extinction spectra with reaction time as parameter, (c) kinetics of degradation (extinction taken at 227 nm) and (d) extent of mineralization by COD and TOC.

without any treatment and the catalytic activity of reused catalyst was found to be same as the original catalyst even after 250 h reactions.

4. Conclusions

The AFM images show vertically grown twisted spindle-shape nanostructured grains providing adequate surface area useful to photocatalytic activity. Mössbauer spectra of photocatalyst demonstrate an asymmetrical sextet with broadened lines and quadrupolar components. The photocatalytic oxidation of salicylic acid and 4-CP in aqueous solutions (showing first order kinetics) using Fe_2O_3, $AlFe_2O_3$, TiO_2/Fe_2O_3 and $TiO_2/AlFe_2O_3$ photocatalysts under sunlight have been studied. The improvement caused by the TiO_2 coating was attributed to the formation of $TiO_2/AlFe_2O_3$ heterojunction resulting in the charge transferring between the photoexcited $AlFe_2O_3$ and TiO_2. According to the performance of $TiO_2/AlFe_2O_3$ catalyst shows a best consistent candidate for degradation of any organic molecules.

Acknowledgment

The authors are very much thankful to Defense Research and Development Organization (DRDO), New Delhi, for the financial support through its project no. ERIP/ER/0503504/M/01/1007.

References

[1] H. Lim, J. Lee, S. Jin, J. Kim, J. Yoon, T. Hyeon, Chem. Commun. (2006) 463–465.
[2] C. Gonzâlez-Arellano, J.M. Campelo, D.J. Macquarrie, J.M. Marinas, A.A. Romero, R. Luque, ChemSusChem 1 (2008) 746–750.
[3] T. Zeng, W.W. Chen, C.M. Cirtiu, A. Moores, G. Song, C.J. Li, Green Chem. 12 (2010) 570–573.
[4] T.S. Kim, J.K. Kim, K. Choi, M.K. Stenstrom, K.D. Zoh, Chemosphere 62 (2006) 926–933.
[5] F.D. Ollis, H. Al-Ekabi (Eds.), Photocatalytic Purification and Treatment of Water and Air, Elsevier Science, Amsterdam, 1993.
[6] S. Kohtani, M. Tomohiro, K. Tokumura, R. Nakagaki, Appl. Catal. B: Environ. 58 (2005) 265–272.
[7] V. Nadtochenko, N. Denisov, O. Sarjusiv, D. Gumy, C. Pulgarin, J. Kiwi, J. Photochem. Photobiol. A: Chem. 181 (2006) 401–407.
[8] Y. Liu, X. Wang, F. Yang, X. Yang, Micropor. Mesopor. Mater. 114 (2008) 431–439.
[9] M.A. Gondal, A. Hameed, Z.H. Yamani, A. Suwaiyan, Appl. Catal. A: Gen. 268 (2004) 159–167.
[10] K.L. Hardee, A.J. Bard, J. Electrochem. Soc. 123 (1976) 1024–1026.
[11] F.B. Li, X.Z. Li, C.S. Liu, T.X. Liu, J. Hazard. Mater. 149 (2007) 199–207.
[12] J. Bandara, K. Tennakone, J. Kiwi, Langmuir 17 (2001) 3964–3969.
[13] T. Kawahara, K. Yamada, H. Tada, J. Colloid Interface Sci. 294 (2006) 504–507.
[14] J. Bandara, U. Klehm, J. Kiwi, Appl. Catal. B: Environ. 76 (2007) 73–81.
[15] Y. Wang, C.S. Liu, F.B. Li, C.P. Liu, J.B. Liang, J. Hazard. Mater. 162 (2009) 716–723.
[16] R. Asahi, T. Morikawa, T. Ohwaki, K. Aoki, Y. Taga, Science 293 (2001) 269–271.
[17] W. Ren, Z. Ai, F. Jia, L. Zhang, X. Fan, Z. Zou, Appl. Catal. B: Environ. 69 (2007) 138–144.
[18] C. Burda, Y. Lou, X. Chen, A.C.S. Samia, J. Stout, J.L. Gole, Nano Lett. 3 (2003) 1049–1051.
[19] M.K. Seery, R. George, P. Floris, S.C. Pillai, J. Photochem. Photobiol. A 189 (2007) 258–263.
[20] L.C. Chen, Y.C. Ho, W.S. Guo, C.M. Huang, T.C. Pan, Electrochim. Acta 54 (2009) 3884–3891.

[21] G. An, W. Ma, Z. Sun, Z. Liu, B. Han, S. Miao, Z. Miao, K. Ding, Carbon 45 (2007) 1795–1801.
[22] F. Mazille, T. Schoettl, C. Pulgarin, Appl. Catal. B: Environ. 89 (2009) 635–644.
[23] F.S. Zhang, H. Itoh, Chemosphere 65 (2006) 125–131.
[24] Q. Ling, J. Sun, Q. Zhou, Q. Zhao, H. Ren, J. Photochem. Photobiol. A: Chem. 200 (2008) 141–147.
[25] X. Zhang, L. Lei, Appl. Surf. Sci. 254 (2008) 2406–2412.
[26] J.K. Leland, A.J. Bard, J. Phys. Chem. 91 (1987) 5076–5083.
[27] M.D. Nikolaki, C.N. Zerva, C.J. Philippopoulos, Appl. Catal. B: Environ. 90 (2009) 89–98.
[28] Z. Ambrus, K. Mogyorosi, A. Szalai, T. Alapi, K. Demeter, A. Dombi, P. Sipos, Appl. Catal. A: Gen. 340 (2008) 153–161.
[29] B. Nanzai, K. Okitsu, N. Takenaka, H. Bandow, Y. Maeda, Ultrason. Sonochem. 15 (2008) 478–483.
[30] S.S. Shinde, A.V. Moholkar, J.H. Kim, K.Y. Rajpure, Surf. Coat. Technol. 205 (2011) 3567–3577.
[31] S.S. Shinde, R.A. Bansode, C.H. Bhosale, K.Y. Rajpure, J. Semicond. 32 (2011) 013001.
[32] S.S. Shinde, S.S. Meena, S.M. Yusuf, K.Y. Rajpure, J. Phys. Chem. C 115 (2011) 3731–3736.
[33] O. Akhavan, R. Azimirad, J. Phys. D: Appl. Phys. 42 (2009) 065404.
[34] L.F. Cortical, S.C. Zapata, S.N. de Medeiros, I.A. dos Santos, A. Peasant Jr., J.B.M. ad Conga, Solid State Ionics 171 (2004) 283.
[35] G.B. Andreozzi, F. Bosi, M. Longo, Am. Mineral. 93 (2008) 658–666.
[36] K. Bachari, J.M.M. Millet, P. Bonville, O. Cherifi, F. Figueras, J. Catal. 249 (2007) 52–58.
[37] G.H. Rossetti, E.D. Albizzati, O.M. Alfano, Ind. Eng. Chem. Res. 41 (2002) 1436–1444.
[38] U.I. Gaya, A.H. Abdullah, J. Photochem. Photobiol. C: Rev. 9 (2008) 1–12.
[39] K. Ishibashi, A. Fujishima, T. Watanabe, K. Hashimoto, J. Photochem. Photobiol. A: Chem. 134 (2000) 139–142.
[40] U.I. Gaya, A.H. Abdullah, Z. Zainal, M.Z. Hussein, J. Hazard. Mater. 168 (2009) 57–63.